Supported Organoiridium-Pincer Catalysts for the Non-Oxidative Dehydrogenation of High-Density Polyethylene

*Samuel B Hunt[a], Jessica V. Lamb[a], Maria Voccia[b], Martina Morello[c,d], David M. Kaphan[a], A. Jeremy Kropf[a], Sergio Tosoni[b], Frédéric A. Perras[e,f], Massimiliano Delferro[a,f]**

[a]Chemical Sciences and Engineering Division, Argonne National Laboratory, Lemont, Illinois 60439, United States

[b]Dipartimento di Scienza dei Materiali, Università Milano-Bicocca, via R. Cozzi, 55 I-20125 Milano, Italy

[c]Department of Chemistry, Biology and Biotechnology, University of Perugia, via Elce di Sotto 8, 06123, Perugia, Italy

[d]Department of Industrial Engineering, University of Padua, via Gradenigo, 6/a, 35131, Padova, Italy

[e]Chemical and Biological Sciences Division, Ames National Laboratory, Ames Iowa 50011, United States

[f]Department of Chemistry, Iowa State University, Ames, Iowa 50011, United States

Corresponding author: delferro@anl.gov (M. D.)

KEYWORDS. Surface Organometallic Chemistry, Polyethylene, Solid State NMR, Non-Oxidative Dehydrogenation, DFT.

ABSTRACT. The iridium-pincer complex {*p*-OP(^{t}Bu)$_2$-C$_6$H$_2$-2,6-OP(^{t}Bu)$_2$]$_2$}Ir(C$_2$H$_4$) (^{P}[Ir]) has been reported as a stable and active catalyst towards alkane dehydrogenation in homogeneous and supported heterogeneous systems.[1-4] Dehydrogenation has been demonstrated as a practical method towards functional polyolefins as a key reactive intermediate where dehydrogenated high-density polyethylene (deHDPE) has been demonstrated as a valuable synthon for upcycling as orthogonal C–H strategies are key to end-of-life upcycling.[5-8] The heterogenization ^{P}[Ir] on metal oxides (SiO_2, Al_2O_3, TiO_2; ^{P}[Ir]/E_yO_x) yields a mixture of organometallic Ir-fragments with catalytic nonoxidative dehydrogenation activity dictated by the binding modes of the organometallic on the surface. When the fragment binds through the ligand, the organoiridium is active, with amount of internal olefin up to 1.23 mol% internal olefins catalyzed at 200 °C under dynamic vacuum. On the other hand, when the organoriridium is bounded though the metal center (Ir-O_{SiO}, the material is catalytically inactive. This was demonstrated via a combination of solid-state NMR and XAFS analysis and supported by DFT calculations. Furthermore, catalytic activity of ^{P}[Ir]/SiO_2 showed comparable reactivity with the homogeneous analogue under the same catalytic conditions up to three cycles. This work highlights the importance of understanding how organometallic precursors react with hydroxylated metal oxide surfaces to establish structure-property relationships.

1. Introduction

Plastic materials are the fastest growing synthetic material industry in the world by volume with annual productions increasing unabated and global production estimated to exceed 1000 million tons by 2050.[9] The rate of production for virgin plastic resin is expected to double by 2040[10, 11] while the total production of plastic is projected to account for 20% of all petroleum.[12, 13] Upcycling strategies that chemically modify waste plastic to improve end-of-life management have emerged as potential solutions. Recently, work into identifying readily achievable synthetic handles has been shown by Winey[14-17], Delferro[6, 7], Sadow[18], and Hartwig[19] for material variation from simple feedstocks with disparate properties (**Figure 1A**).[5, 20] Among these, dehydrogenated polyethylene has demonstrated significant value as a chemical handle, with synthetic modification realizing novel polar, fluoroalkylated, telechelic macromonomers, and esterified materials that possess highly tunable and controllable properties that increases the depth of end-of-life strategies (**Figure 1A**).[5-7, 14-17, 21] Dehydrogenated polyethylene has been synthesized in a variety of methods,[22, 23] however, non-oxidative, acceptor-less, Ir-pincer complexes have shown remarkable tunability and control, with no side product and high reaction fidelity towards maintaining molecular weight.[1, 3, 5-7]

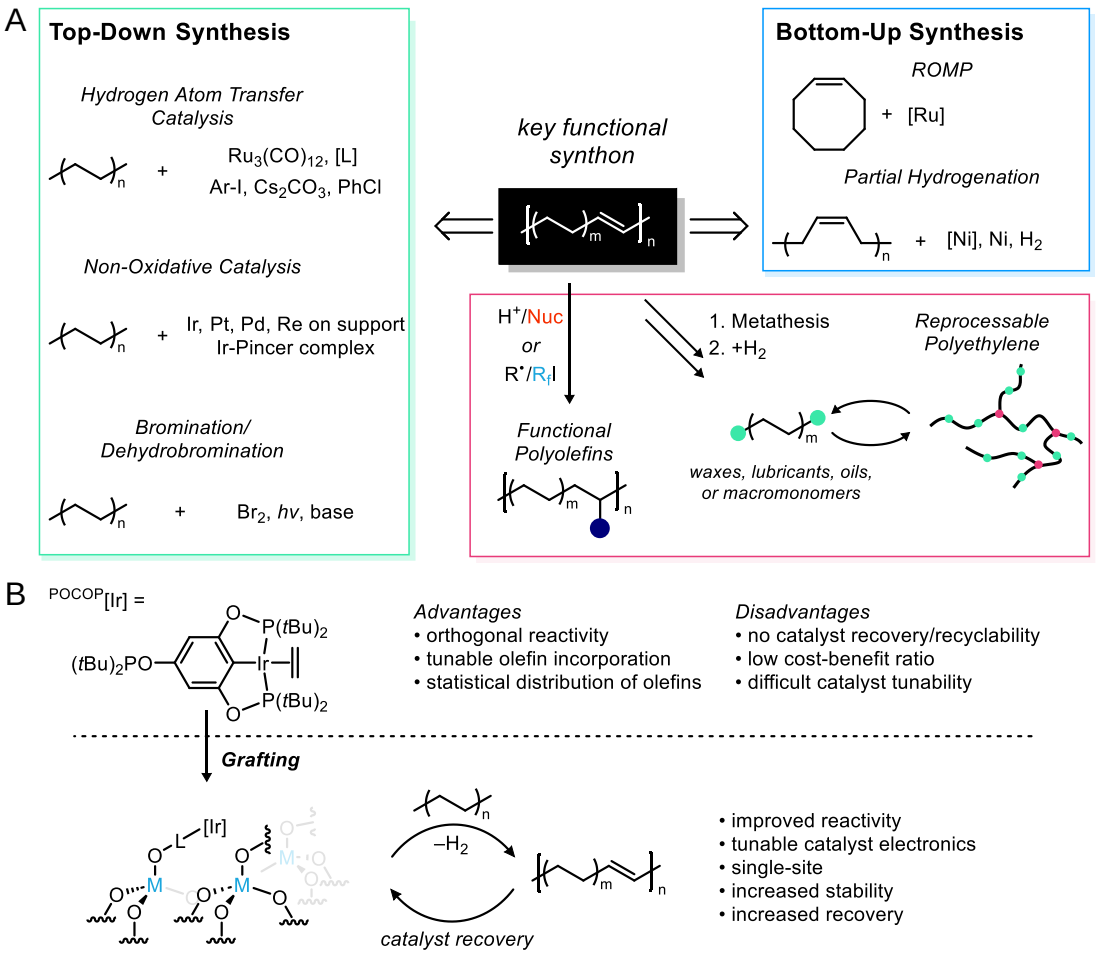

Figure 1. (A) Prior work on waste plastic dehydrogenation and chemical differentiation.[5, 14-17, 21, 23-25] (B) SOMC grafting and improved polymer dehydrogenation strategy.

Dehydrogenation of alkanes is highly attractive as a method to introduce olefin into otherwise inert species owing to the more reactive nature of alkenes and the availability of the chemical transformations available to them. Iridium-pincer complexes have been well developed in the literature over the past thirty years as catalysts for the selective and nonoxidative C–H dehydrogenation of aliphatic bonds. In particular, their ubiquity and robustness towards long-chain and heavier alkanes has been reported where their high selectivity is greatly desired where the presence of H_2 acceptors can induce the formation of terminal olefins.[26, 27] This control is greatly

desired for a variety of transformations, like the synthesis of α-olefins from heavier alkanes as precursors to surfactants and detergents where terminal functionalization control is required.[26-28] However, the ability to form internal olefins and perform statistical random walking is valuable for synthesizing dehydrogenated polyolefins that are readily modified to a variety of upcycled materials.[5-7]

Current literature for Ir-pincer catalyzed polyolefin dehydrogenation has focused exclusively on homogeneous processes, which detract the overall efficacy and limit catalyst recyclability. Increasing the catalyst recovery by supporting the catalytically active organometallic species on a heterogeneous support would mitigate costs, improve reactivity, and increase recovery. Supported Ir organometallic species have been reported in the literature for a variety of surfaces and ligands,[29-31] however limited efforts have been afforded to probe the binding mode, the scope of alkanes, particularly with high melt viscosity polyolefins, and understand their recycling in such systems. An earlier report by Celik et al. showed the versatility for continuous flow-butane dehydrogenation using supported Ir-pincer catalysts with excellent thermal stability and activity with limited exploration of the binding modes.[2] Given this and prior reports, this work (**Figure 1B**) demonstrates the viability and improved reactivity of supported Ir-pincer complexes in post-consumer high-density polyethylene (HDPE) dehydrogenation with an increase in reactivity over homogeneous catalyst reports.[5] Solid-state ^{1}H, ^{13}C, and ^{31}P NMR analysis and XAS, supported by Density Functional Theory (DFT) calculations, elucidated the structure of the active catalyst species.

2. Results and Discussion

2.1. Preparation of ^{Z}[Ir]/E_xO_y Catalysts and Grafting. Iridium pincer complexes {*p*-OP(^{t}Bu)$_2$-C_6H_2-2,6-OP(^{t}Bu)$_2$]$_2$}Ir(C_2H_4) (^{P}[Ir]) and {C_6H_2-2,6-OP(^{t}Bu)$_2$]$_2$}Ir(C_2H_4) (^{H}[Ir]) were synthesized according to previous literature procedure.[4] Note that ^{H}[Ir] was used a model complex due to the inability to bind through the ligand to the surface. The general procedure for grafting was performed identically for both catalysts; ^{Z}[Ir] (z = OP9tBu) or H) was grafted onto E_xO_y (E_xO_y = SiO_2, Al_2O_3 or TiO_2) with a mass ratio of 1:30 to obtain ^{Z}[Ir]/E_xO_y (**Figure 2**). In both systems, namely, ^{P}[Ir] and ^{H}[Ir], the metal can oxidatively insert into a surface hydroxyl, leading to the formation of a trivalent iridium hydride (**Figure 2** ^{P}[Ir]$_M$/E_xO_y and ^{H}[Ir]$_M$/E_xO_y, respectively). In addition, in the case of ^{P}[Ir], the support may also react at the *para* position of the POCOP ligand, releasing a free dialkylphine oxide, yielding ^{P}[Ir]$_L$/E_xO_y.[2, 32] Note that SiO_2 (Davisil, grad 646) was calcined under flowing air at 700 °C for 3 hours, while TiO_2 (anatase) was calcined at 200 °C under flowing air for 12 hours followed by treatment under vacuum at 200 °C for 12 hours; γ-Al_2O_3 was dried under vacuum at 200 °C overnight as pretreatment. Catalysts were grafted via shaking (400rpm) 10 mg of catalysts with 300 mg of support in toluene at room temperature for one hour.

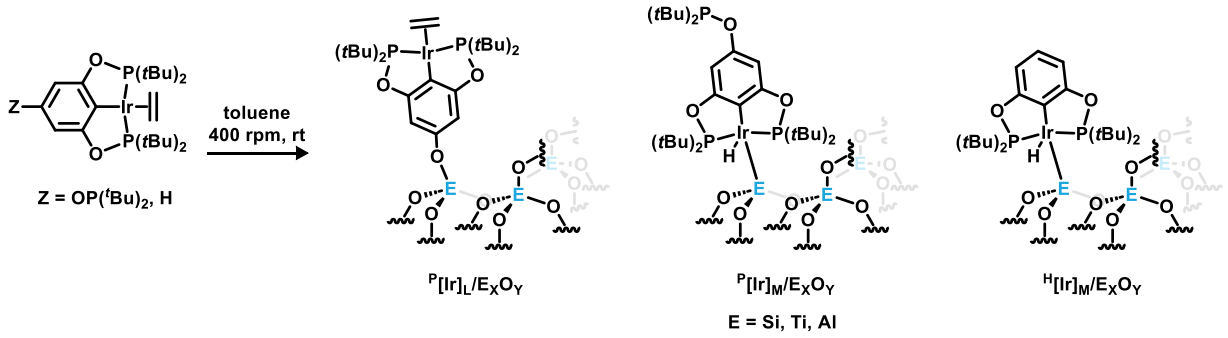

Figure 2. Generic Ir-organometallic complex and specific supported Ir catalysts with the possible binding modes.

Dehydrogenations were performed by charging a Schlenk flask with HDPE (150 mg) and supported catalysts (500 mg) with toluene (2 mL) as a plasticizer. The reaction was heated and stirred at 120 °C until the polymer turned homogeneous. The sample was cooled to room temperature then evacuated under dynamic vacuum and brought to 200 °C for 18 hours. After reacting, the mixture was solubilized with toluene at 120 °C (approximately 50 mL of toluene per gram of polymer) and precipitated into methanol under vigorous stirring. This was repeated in triplicate and the final deHDPE dried under vacuum. For recyclability studies, the reaction mixture was worked up under an argon atmosphere and the dried catalyst used directly in further reactions.

2.2. Catalyst Characterization. Supported catalysts were characterized via Inductively Coupled Plasma Optical-Emission Spectroscopy (ICP-OES) analysis and revealed lower iridium loadings for $^{H}[Ir]/E_xO_y$ than $^{P}[Ir]/E_xO_y$ (Table 1). Additionally, lower iridium content was observed for $^{P}[Ir]/Al_2O_3$ and $^{P}[Ir]/TiO_2$ compared to $^{P}[Ir]/SiO_2$.

Table 1. ICP-OES data for $^{Z}[Ir]/E_xO_y$

Catalyst	Color	Ir (wt%)
$^{H}[Ir]/SiO_2$	Orange	0.381
$^{P}[Ir]/SiO_2$	Red	0.623
$^{H}[Ir]/Al_2O_3$	Pale Orange	0.037
$^{P}[Ir]/Al_2O_3$	Pale Pink	0.572
$^{H}[Ir]/TiO_2$	Pale Red	0.373
$^{P}[Ir]/TiO_2$	Paled	0.584

Solid-state NMR experiments that leveraged either ^{1}H-detection under fast-magic-angle spinning (fast-MAS) or dynamic nuclear polarization (DNP)[33, 34] for surface sensitization were applied to gain clarity on the surface binding modes.

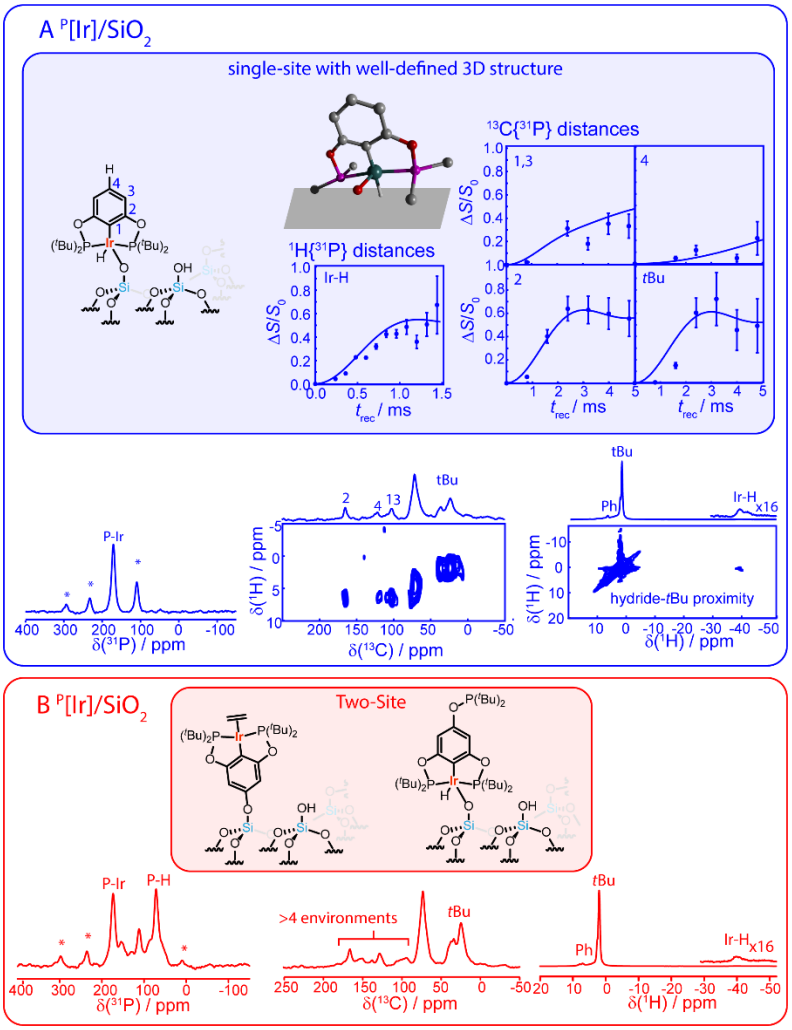

Figure 3. NMR analysis of ^{H}[Ir]/SiO_2 (A) and ^{P}[Ir]/SiO_2 (B). (A) DNP-enhanced ^{31}P CPMAS and ^{13}C{^{1}H} HETCOR spectra display resonances from a single unique site. A ^{1}H fast-MAS RFDR spectrum further displays a well-resolved Ir hydride signal that correlates with the ^{t}Bu from the POCOP ligand. ^{13}C{^{31}P} and a ^{1}H{^{31}P} S-REDOR distances agree with the 3D configuration from the expected single-site. (B) A complex DNP-enhanced ^{13}C CPMAS NMR spectrum is only consistent with multiple surface sites. This is confirmed by ^{1}H and ^{31}P NMR that display both the dislocation of the *para* phosphinite and the formation of an Ir(III) hydride.For ^{H}[Ir]/SiO_2 (**Figure 3A**) the ^{31}P NMR spectrum shows a single species consistent with both phosphinites remaining bound to Ir. In conjunction, it was observed the formation of a hydride consistent with oxidative

insertion and direct Ir-surface bonding. The ^{13}C NMR spectrum agrees with related compounds in literature,[4, 32] further suggesting the single site nature of the organoiridium. This assignment is confirmed using distance measurements between ^{1}H and ^{13}C to ^{31}P using S-REDOR[35] and REDOR[36] experiments, respectively. These data are in remarkable agreement with the expected 3D structure from DFT calculations (*vide infra*, **Figure 3A**) for the site, after considering the dynamics of the hydride bonding. A ^{1}H homonuclear single-quantum correlation spectrum acquired using fpRFDR mixing[37, 38] further confirmed that the hydride species is near the ^{t}Bu groups and a part of the same molecule.

In the case of $^{P}[Ir]/SiO_2$ (**Figure 3B**) the release *para* phosphinite and the formation of an Ir(III) hydride were observed $^{P}[Ir]_{\mathbf{M}}/SiO_2$, suggesting that both binding modes are present. The observed hydride resonance of $^{P}[Ir]_{\mathbf{M}}/SiO_2$ is lower in magnitude than that seen in $^{H}[Ir]_{\mathbf{M}}/SiO_2$ along with a more complex aromatic region in the DNP-enhanced ^{13}C CPMAS NMR spectrum. This is consistent with a multi-site nature of the catalyst. The amount of hydride formation was also studied as a function of grafting time (15 minutes, 2 hours, and 18 hours), where the amount of hydride was unaffected. However, more of the phosphine oxide product was observed at increased grafting time (18 hours), suggesting possible decomposition. The integration of the relative intensity of the ^{t}Bu and hydride signals in the ^{1}H CPMAS NMR spectra gave ratio of 58:42 for $^{P}[Ir]_{\mathbf{L}}/SiO_2$: $^{P}[Ir]_{\mathbf{M}}/SiO_2$.

X-Ray Absorption Fine Structure (XAFS) spectroscopy was performed at the Ir L3 edge (**Figure 4B-F**) to validate the structure and existence of the ^{P}[Ir] ligand framework **(Figure 4A**) upon chemisorption and at elevated temperature in butane to understand the organometallic stability in relevant catalytic conditions. The X-ray absorption near edge structure is shown in **Figure 4B-C**. The precursor spectra are similar, as expected if the difference in structure is in the *para* position,

more than 0.6 nm away from the Ir atom. After chemisorption on SiO_2, both supported Ir spectra show the same change in the post edge region, shown more clearly in **Figure 4B**, with a small peak at 11240 eV that persists after the catalytic reaction. **Figure 4D-E** compares the EXAFS Fourier transforms of the supported complexes to the precursors. Qualitatively this indicates a retention of the pincer ligand after binding to the surface. A fit of the precursor compounds indicated an Ir–P bond length of 2.281 Å that does not change significantly after binding and may increase by only 0.009 Å after catalysis (**Table S2, Figure S16**). The fit of $^{H}[Ir]/SiO_2$ is shown in **Figure 4E**. The k^3 weighting and k range to 16.5 $Å^{-1}$ in this figure significantly suppresses the Ir–C peak compared to the Ir–P peak, although the fitting was done with simultaneous k^1, k^2, and k^3 weightings to increase the sensitivity to the weaker Ir–C scattering. Although the data range for the supported complex is too small to fully resolve the two scattering paths a Cauchy wavelet transformation (**Figure 4G**) resolves the presence of the Ir–C and Ir–P paths at lower-k/lower-R, and higher-k/higher-R, respectively. The EXAFS fits and the Cauchy wavelet transform both suggest a lower Ir-C coordination number for $^{H}[Ir]_M/SiO_2$ complex, due to the loss of the ethene ligand and the concomitant formation of an Ir^{3+}-O bond and Ir-H bond (*vide supra* SS NMR).

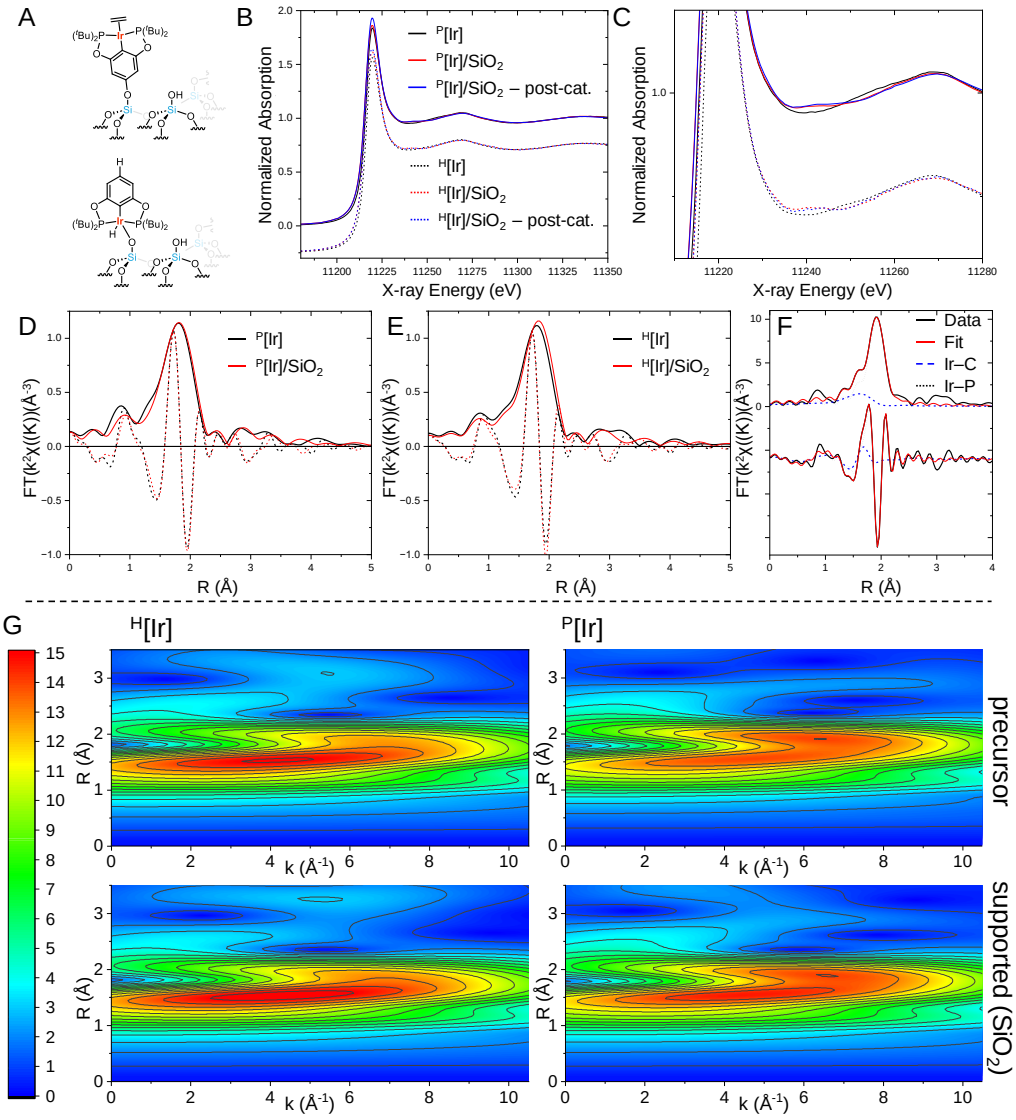

Figure 4. (A) Structures of supported ^{P}[Ir] and ^{H}[Ir]; (B) full y-axis X-ray absorption near edge structure (XANES) of supported catalysts; (C) zoomed in y-axis XANES of supported catalysts; (D) comparison of the FT of the precursor and supported ^{P}[Ir] (FT k range: 3.0 – 10.5 Å^{-1}, k^2 shown); (E) comparison of the FT of the precursor and supported ^{H}[Ir]; (F) EXAFS fig of ^{H}[Ir] using Ir–C and Ir–P scattering paths (FT k-range: 3.0 – 16.5 Å^{-1}, k^3 shown, fit R range: 1.2 – 2.6 Å); (G) Cauchy Wavelet Transformation. Cauchy wavelet transformation of the EXAFS spectra (k$^{1.5}$ weighting, k range: 0 – 10.5 Å^{-1}, R range: 0 – 7 Å). The contour maps are on the same arbitrary

scale to more easily compare intensities between images. Fit results are shown in **Table S2** (Fourier transform magnitude: upper traces; real component of the FT: lower offset traces).DFT calculations were performed to analyze the binding modes of the supported complexes, on amorphous SiO_2 (Details are provided in SI). Calculations show that the formation of both structures of the supported catalysts, $^{P}[Ir]_{\mathbf{M}}/SiO_2$ and $^{P}[Ir]_{\mathbf{L}}/SiO_2$, are exothermic with respect to the gas-phase complex and the clean SiO_2 surface, with ΔE = -196.83 kJ mol^{-1} for Ir-bound species and -76.22 kJ mol^{-1} for *para*-O bound species.[2] To probe the formation of the supported catalyst, structural relaxations were commenced by treating the pincer complex and unbound support as freely interacting. In the case of *para*-O binding, a relevant finding is that no stable, intact structure was detected between the *para*-phosphinite group and the surface, even when starting from the undissociated $^{P}[Ir]$ complex interacting with the silica surface via a Si–O–P–O bridge. Fragmentation spontaneously takes place on the O–C bond, leaving the complex bound via a Si–O–C (**Figure S11B**), and the leaving (^{t}Bu)$_2$PH group that interacts with a siloxane group, further confirming the formation of the majority species (**Figure 3**). Calculations also showed that the ethylene coordination to the organometallic $^{P}[Ir]$ facilitates the formation of the $^{P}[Ir]_{\mathbf{L}}$ where the binding energy of $^{P}[Ir]_{\mathbf{M}}$ to ethylene is -9.65 kJ mol^{-1} and the binding energy of $^{P}[Ir]_{\mathbf{L}}/SiO_2$ to ethylene is -173.67 kJ mol^{-1} (**Figure S14)**. These calculations were performed by simulating the coordination of ethylene on the two different binding modes for the grafted organometallic $^{P}[Ir]/SiO_2$. This suggests that a highly reactive and unhindered iridium center will preferentially react with the surface to form an Ir surface bound $^{P}[Ir]_{M}/SiO_2$ complex, where hydride species can form stable bonds with the Ir centre. In turn, $^{P}[Ir]_{M}/SiO_2$ will only weakly interact with ethylene, but may play a role in dissociating hydrogen.[2] Viceversa, if a free Pincer complex binds ethylene with its Ir centre before binding silica, the coordination to the surface will preferentially take place

via the para-O atom. This supports the solid-state ^{31}P NMR analysis where the ^{Z}[Ir]/SiO_2 species has a minority of Ir-bound versus *para*-O bound species. The shorter C–Ir distances of the ethylene to the active site (2.28/2.26 Å for $^{P}[Ir]_M/SiO_2(C_2H_4)$ and 2.20/2.19 Å for $^{P}[Ir]_L/SiO_2(C_2H_4)$, **Figure S14**), as well as the larger negative charge on the ethylene for $^{P}[Ir]_L/SiO_2(C_2H_4)$ than $^{P}[Ir]_M/SiO_2(C_2H_4)$ (Q = -0.09 and -0.21 |e| for $^{P}[Ir]_M/SiO_2(C_2H_4)$ and $^{P}[Ir]_L/SiO_2(C_2H_4)$, respectively, with a charge of Q = 0.00 for C_2H_4) certifies a stronger activation of the monomer for $^{P}[Ir]_L/SiO_2(C_2H_4)$ than $^{P}[Ir]_M/SiO_2(C_2H_4)$, due to the σ donation from the ethylene to the metal center and to the π retrodonation from the metal to the ethylene. This is also confirmed by the density of states (DOS) plot in **Figure S15** (up, right). Furthermore, it also emerges the Ir (5*d*) states fall in the wide silica gap (Figure S15). The lowest unoccupied molecular orbital (LUMO) of ethylene is very close to the conduction band edge of silica, while its HOMO is strongly hybridized with the substrate in $^{P}[Ir]_M/SiO_2(C_2H_4)$, and much less in $^{P}[Ir]_L/SiO_2$, confirming the stronger coordination and greater activation of the ethylene for $^{P}[Ir]_L/SiO_2(C_2H_4)$ than $^{P}[Ir]_M/SiO_2(C_2H_4)$

2.3. Catalytic Dehydrogenation. Dehydrogenation reactions were conducted in a Schlenk flask with 150 mg shredded post-consumer HDPE water jug (M_n = 13.2 kg mol^{-1}, $Đ$ = 4.7, **Entry 1**) without any further purification, 500 mg $^{Z}[Ir]/E_xO_y$ (0.00162 mmol), and ~2 mL toluene to act as a plasticizer and aid mixing. Initially, the flask was sealed and heated at 120 °C to facilitate polymer and catalyst mixing. The flask was then opened to dynamic vacuum, heated to 200 °C, and stirred for 24 hours.

Table 1. Nonoxidative catalytic dehydrogenation of waste HDPE

Entry	Catalyst	Ir (mmol)	HDPE (mg)	HDPE:Ir [b]	Sieve Size (μm)	Olefin (mol%)[c]	M_n (kg mol^{-1})[d]	$Đ$[d]
1	–				–	0.11[f]	13.2	4.7
2	^{P}[Ir][g]	0.003470	300	3081:1	–	0.46	15.1	4.5
3	^{P}[Ir]/TiO_2[e]	0.003762	150	1421:1	–	0.11	6.9	4.8
4	^{P}[Ir]/Al_2O_3	0.014879	150	359:1	–	0.28	11.8	4.0
5	^{H}[Ir]/SiO_2	0.009911	150	539:1	–	0.26	53.1	1.48
6	^{P}[Ir]/SiO_2	0.016127	150	331:1	–	0.86	7.7	8.5
7	^{P}[Ir]/SiO_2	0.016127	150	331:1	177	1.23	10.2	2.9
8	^{P}[Ir]/SiO_2	0.008064	150	663:1	177	0.49	9.1	5.7
9	^{P}[Ir]/SiO_2	0.008064	150	663:1	144	0.55	12.8	4.3
10	^{P}[Ir]/SiO_2	0.008064	150	663:1	125	0.60	13.0	3.8
11	^{P}[Ir]/SiO_2	0.003225	150	1658:1	177	0.45	10.6	5.9
12	^{P}[Ir]/SiO_2	0.001774	150	3013:1	177	0.42	9.2	5.7
13	^{P}[Ir]/SiO_2[f]	0.007096	600	3013:1	177	0.45	7.3	21

[a]Conditions: HDPE jug (150 mg), catalyst (500 mg), 24 h, 200 °C, vacuum, toluene as a plasticizer, [b]Determined by ICP-OES, [c]Number of ethylene repeat units, determined by ^{1}H NMR spectroscopy, [d]Determined by high-temperature gel permeation chromatography in 1,2,4-$C_6H_3Cl_3$ at 150°C versus polyethylene standards, [e]75 mg HDPE jug, [f]600 mg HDPE jug, [g]75 mg HDPE jug. [f]Terminal olefin already present in the starting HDPE.

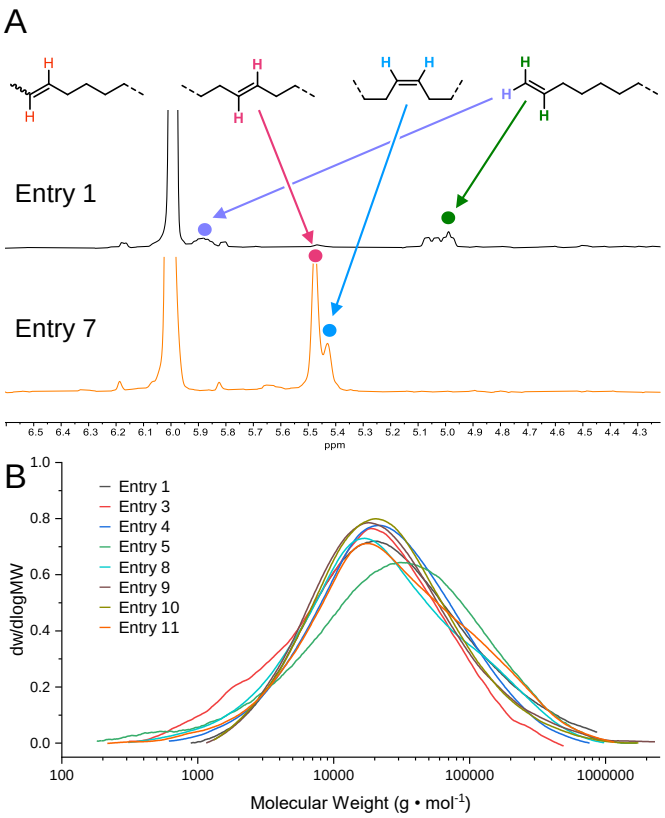

Figure 5. (A) ^{1}H NMR analysis of selected dehydrogenated HDPE and parent waste HDPE with small amount of terminal olefin from chain termination during polymerization (0.13 mol%); (B) SEC analysis of dehydrogenated polyethylene.

The dehydrogenated high-density polyolefin samples (de-HDPE) were then characterized by high temperature solution phase NMR and GPC to determine the degree of dehydrogenation (**Figure 5A-B**) and molecular weight, respectively. The number of olefins was calculated per constitutional repeat unit via ^{1}H NMR analysis relative to the aliphatic region comprising the saturated polymer on the assumption that the degree of olefination is significantly less than the total degree of polymerization (see SI equation 1).[5] studies of the catalysts showed that when normalizing for the amount of Ir, the ^{P}[Ir]/SiO_2 catalysts was most active. The effect of reduced catalyst amount on dehydrogenation was also studied, where a linear decrease in internal olefins was observed

between 0.0161 and 0.0042 mmol of Ir. To probe mass transport considerations in the polymer melt, the influence of grinding and sieving ^{P}[Ir]/SiO_2 catalyst was also studied. Three size sizes were employed (≤177, ≤144, and ≤125 μm) with ^{P}[Ir]/SiO_2:PE of 250:150. Initially, a sieve size of ≤177 μm was employed, leading to an 80% increase in internal olefins compared to the un-sieved catalyst (increase in internal olefins from 0.62 to 1.11 mol%). A small increase in olefin content was observed in the dehydrogenated products with decreased sieve size (0.56, 0.53, and 0.49 mol% for ≤125, ≤144, and ≤177 μm, respectively; Table 1), this is surmised to derive from the ability of the polymer chain to fully envelop smaller particles, thereby increasing contact with the active sites.[39] Interestingly, when matched for the amount of iridium, the homogeneous and heterogeneous reactions showed similar activities (0.46 and 0.45 mol% internal olefins with Ir:polymer of 1:450). Note also that scale (×4) also did not affect activity with ~0.45 mol% olefins obtained with both 150 and 600 mg HDPE. The NMR spectra show the expected CH_2 backbone, CH_3 end groups, and internal olefin resonances (**Figure 5A**). The products from these reactions show unimodal molecular weight distributions with M_w and M_n within error margins of the starting material,[40] consistent with no chain scission occurring during catalysis, as shown in **Figure 5B**. [41-43]

2.4. Catalyst Recyclability and Post-Catalysis Analysis. Post-catalysis ^{13}C and ^{31}P NMR analysis showed a significant amount of leftover polyethylene and trapped toluene coating the catalyst (**Figure 6A**, left). Notably, the ^{31}P NMR analysis demonstrated no significant change in the ligand framework after post-catalysis indicating that the organometallic species was intact. Despite the significant polyethylene carryover from reaction to reaction, ^{P}[Ir]/SiO_2 (**Figure 6B**) demonstrated remarkable recyclability considering the significant amount of polyethylene unable to be removed. As the catalyst was continually reused, the reactivity decreased linearly, plausibly

due to the buildup of polymer on the surface from reaction to reaction (**Figure 6A**). It should be noted that the buildup of polyethylene is unavoidable due to the high chemical stability and insolubility of HDPE; furthermore, the final product, dehydrogenated HDPE may also be present where further work on developing flow-beds may improve reactivity and catalyst recyclability.

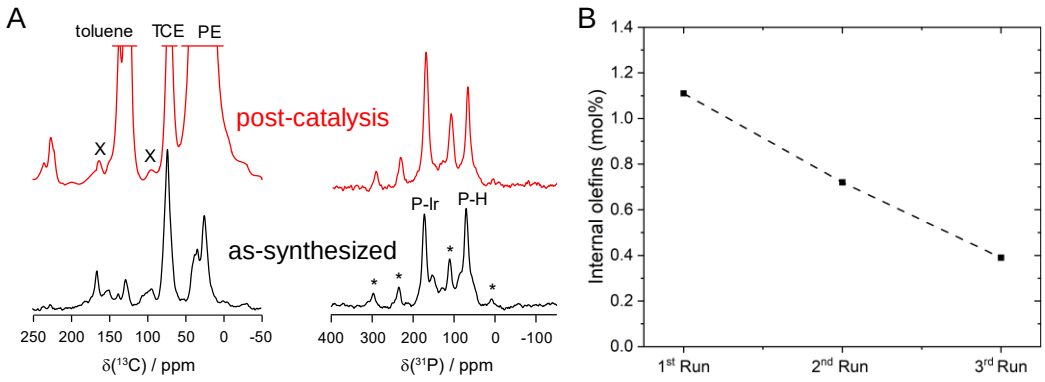

Figure 6. (A) solid-state ^{31}P and ^{13}C catalysts before and after dehydrogenation reaction; (D) ^{P}[Ir]/SiO_2 recyclability studies. Conditions: HDPE jug, ^{P}[Ir]/SiO_2 catalyst 24 h, 200 °C, vacuum, toluene as a plasticizer.

3. Conclusion

A comprehensive study was demonstrated using Ir-Pincer dehydrogenation catalysts supported on an array of surfaces for HDPE valorization. SiO_2 surfaces that were subjected to molecular sieving to increase surface area increased the reactivity of Ir-pincer over less acidic surfaces (SiO_2 > Al_2O_3 > TiO_2). Critically, the extension to supported Ir-Pincer complexes allowed for similar reactivities compared to homogeneous variants. The reactivity did not lead to any side reactions that cleaved or crosslinked polymer chains, with no heterogeneity in the product distribution as analyzed by SEC analysis where no low- or high-molecular weight shoulders were observed. The binding mode of the Ir-pincer catalyst to the surface was explored via solid-state NMR analysis

and by computation. NMR analysis of the ^{P}[Ir]/SiO_2 indicates that the grafting process through the para-oxygen linker generates of mixture of backbone and metal center grafting, whereas with ^{H}[Ir]/SiO_2 catalyst only the Ir center can bond to the surface. The computational analysis agrees with the binding mode presented by the spectroscopic analysis and helps to rationalized future designs of such supported catalysts. This work builds on prior results that demonstrate the vitality of Ir-catalyzed dehydrogenation for linear polyolefin upcycling and enables a rational design for further supported organometallic pincer complexes.

ASSOCIATED CONTENT

Supporting Information.

Experimental procedures, experimental data, material characterization, computational data, NMR, SEC analysis, X-ray Absorption Fine Structure (XAFS) Spectroscopy (PDF).

AUTHOR INFORMATION

Corresponding Author

*Massimiliano Delferro, delferro@anl.gov

Author Contributions

The manuscript was written through contributions of all authors. All authors have given approval to the final version of the manuscript.

Funding Sources

This work was supported as part of the Institute for Cooperative Upcycling of Plastics (iCOUP), an Energy Frontier Research Center funded by the U.S. Department of Energy, Office of Science, Basic Energy Sciences at Argonne National Laboratory and Ames National Laboratory. Argonne National Laboratory is operated by UChicago Argonne LLC under Contract DE-AC-02–06CH11357 for the United States Department of Energy. Ames National Laboratory is operated for the U.S. Department of Energy by Iowa State University under Contract No. DE-AC02-07CH11358. XAS work at Argonne National Laboratory was supported by the U.S. Department of Energy (DOE), Office of Basic Energy Sciences, Division of Chemical Sciences, Geosciences, and Biosciences, Catalysis Science Program under contract No. DE-AC-02-06CH11357. Use of the Advanced Photon Source is supported by the U.S. Department of Energy, Office of Science,

and Office of the Basic Energy Sciences, under Contract No. DEAC02−06CH11357. MRCAT operations are supported by the Department of Energy and the MRCAT member institutions.

Notes

The authors declare no competing financial interest.

ACKNOWLEDGMENT

MV and ST acknowledge financial support from Fondazione Cariplo (grant 2022-0713 PLANET) and supercomputing resources granted by CINECA.

ABBREVIATIONS

HDPE, high-density polyethylene; CAT, catalyzed hydrogen atom transfer; LDPE, low-density polyethylene; LLDPE, linear low-density polyethylene; SOMC, surface organometallic chemistry; DFT, density functional theory; GPC, gel permeation chromatography; NMR, nuclear magnetic resonance; ICP-OES, inductively coupled plasma optical-emission; XAFS, X-ray absorption fine structure; EXAFS, extended X-ray absorption fine structure; XANES, X-ray absorption near edge structure; DOS, density of states; LUMO, low unoccupied molecular orbital; de-HDPE, dehydrogenated high-density polyethylene.

REFERENCES

(1) Ray, A.; Kissin, Y. V.; Zhu, K.; Goldman, A. S.; Cherian, A. E.; Coates, G. W. Catalytic post-modification of alkene polymers: Chemistry and kinetics of dehydrogenation of alkene polymers and oligomers with pincer Ir complexes. *Journal of Molecular Catalysis A: Chemical* **2006**, *256* (1), 200-207. DOI: https://doi.org/10.1016/j.molcata.2006.04.017.
(2) Sheludko, B.; Cunningham, M. T.; Goldman, A. S.; Celik, F. E. Continuous-Flow Alkane Dehydrogenation by Supported Pincer-Ligated Iridium Catalysts at Elevated Temperatures. *ACS Catal.* **2018**, *8* (9), 7828-7841. DOI: 10.1021/acscatal.8b01497.
(3) Ray, A.; Zhu, K.; Kissin, Y. V.; Cherian, A. E.; Coates, G. W.; Goldman, A. S. Dehydrogenation of aliphatic polyolefins catalyzed by pincer-ligated iridium complexes. *Chemical Communications* **2005**, (27), 3388-3390, 10.1039/B502120K. DOI: 10.1039/B502120K.
(4) Huang, Z.; Brookhart, M.; Goldman, A. S.; Kundu, S.; Ray, A.; Scott, S. L.; Vicente, B. C. Highly Active and Recyclable Heterogeneous Iridium Pincer Catalysts for Transfer Dehydrogenation of Alkanes. *Adv. Synth. Catal.* **2009**, *351* (1-2), 188-206. DOI: 10.1002/adsc.200800615.
(5) Arroyave, A.; Cui, S.; Lopez, J. C.; Kocen, A. L.; LaPointe, A. M.; Delferro, M.; Coates, G. W. Catalytic Chemical Recycling of Post-Consumer Polyethylene. *J. Am. Chem. Soc.* **2022**, *144* (51), 23280-23285. DOI: 10.1021/jacs.2c11949.
(6) Hunt, S. B.; Delferro, M. Dehydrogenated Polyethylene from Discarded Plastics as a Synthon for Functional Polyolefins. *ACS Appl. Polym. Mater.* **2024**, *6* (15), 8727-8732. DOI: 10.1021/acsapm.4c01699.
(7) Hunt, S. B.; Román, A. J.; Wang, X.; Perez, J. M.; Perras, F. A.; Lee, B.; Xu, J.; Delferro, M. Fluoropolymer Composites from Partially Perfluoroalkylated Waste Polyethylene. *ACS Appl. Mat. Inter.* **2025**, *17* (22), 33221-33232. DOI: 10.1021/acsami.5c06083.
(8) Williamson, J. B.; Lewis, S. E.; Johnson III, R. R.; Manning, I. M.; Leibfarth, F. A. C−H Functionalization of Commodity Polymers. *Angew. Chem., Int. Ed.* **2019**, *58* (26), 8654-8668. DOI: https://doi.org/10.1002/anie.201810970.
(9) Jehanno, C.; Alty, J. W.; Roosen, M.; De Meester, S.; Dove, A. P.; Chen, E. Y. X.; Leibfarth, F. A.; Sardon, H. Critical advances and future opportunities in upcycling commodity polymers. *Nature* **2022**, *603* (7903), 803-814. DOI: 10.1038/s41586-021-04350-0.
(10) Geddie, J. B., J. *Big Oil's plastic boom threatens U.N.'s 'historic' pollution pact*; Reuters, Reuters, 2022. https://www.reuters.com/business/environment/big-oils-plastic-boom-threatens-uns-historic-pollution-pact-2022-03-04/.
(11) Dokl, M.; Copot, A.; Krajnc, D.; Fan, Y. V.; Vujanović, A.; Aviso, K. B.; Tan, R. R.; Kravanja, Z.; Čuček, L. Global projections of plastic use, end-of-life fate and potential changes in consumption, reduction, recycling and replacement with bioplastics to 2050. *Sustainable Production and Consumption* **2024**, *51*, 498-518. DOI: 10.1016/j.spc.2024.09.025.
(12) Morlet, A. B., J.; Opsomer, R.; Widmer, S.; Banks, I.; De Smet, M.; Murphy, J.; Steventon, P.; Rodger, S.; Waughray, D.; Chalmers, N.; Pennington, J.; Baudoin, L.; Defruyt, S.; Stuchtey, M. R.; Swartz, S.; Vanthournout, H. *The New Plastics Economy — Rethinking the future of plastics*; World Economic Forum, Ellen MacArthur Foundation and McKinsey & Company, 2016. http://www.ellenmacarthurfoundation.org/publications.
(13) Sun, J.; Lee, Y.-H.; Yappert, R. D.; LaPointe, A. M.; Coates, G. W.; Peters, B.; Abu-Omar, M. M.; Scott, S. L. Bifunctional tandem catalytic upcycling of polyethylene to surfactant-range alkylaromatics. *Chem* **2023**, *9* (8), 2318-2336. DOI: 10.1016/j.chempr.2023.05.017.

(14) Ogbu, I. M.; Fastow, E. J.; Winey, K. I.; Kozlowski, M. C. Hydroesterification of Polycyclooctene to Access Linear Ethylene Ethyl Acrylate Copolymers as a Step Toward Polyolefin Functionalization. *Macromolecules* **2024**, *57* (22), 10767-10777. DOI: 10.1021/acs.macromol.4c02074.
(15) John Chethalen, R.; Kim, M.; Ruiz, J. C.; Tu, C.-H.; Gray, J.; Winey, K. I.; Lesser, A. J.; Crosby, A. J.; Coughlin, E. B. Incorporation of Thioacetate Pendants on a Polyalkenamer Enables High Extensibility. *Macromolecules* **2024**, *57* (21), 10358-10367. DOI: 10.1021/acs.macromol.4c02110.
(16) Fastow, E.; Chethalen, R. J.; Coughlin, E. B.; Winey, K. I. Thiol-ene click chemistry incorporates carboxylic acid-terminated alkane pendants on polycyclooctene to tune properties. *Giant* **2024**, *17*, 100231. DOI: 10.1016/j.giant.2023.100231.
(17) Chethalen, R. J.; Fastow, E. J.; Coughlin, E. B.; Winey, K. I. Thiol–ene Click Chemistry Incorporates Hydroxyl Functionality on Polycyclooctene to Tune Properties. *ACS Macro Lett.* **2023**, *12* (1), 107-112. DOI: 10.1021/acsmacrolett.2c00670.
(18) Kanbur, U.; Paterson, A. L.; Rodriguez, J.; Kocen, A. L.; Yappert, R.; Hackler, R. A.; Wang, Y.-Y.; Peters, B.; Delferro, M.; LaPointe, A. M.; et al. Zirconium-Catalyzed C–H Alumination of Polyolefins, Paraffins, and Methane. *Journal of the American Chemical Society* **2023**, *145* (5), 2901-2910. DOI: 10.1021/jacs.2c11056.
(19) Shi, J. X.; Ciccia, N. R.; Pal, S.; Kim, D. D.; Brunn, J. N.; Lizandara-Pueyo, C.; Ernst, M.; Haydl, A. M.; Messersmith, P. B.; Helms, B. A.; Hartwig, J. F. Chemical Modification of Oxidized Polyethylene Enables Access to Functional Polyethylenes with Greater Reuse. *J. Am. Chem. Soc.* **2023**. DOI: 10.1021/jacs.3c07186.
(20) Ciccia, N. R.; Shi, J. X.; Pal, S.; Hua, M.; Malollari, K. G.; Lizandara-Pueyo, C.; Risto, E.; Ernst, M.; Helms, B. A.; Messersmith, P. B.; Hartwig, J. F. Diverse functional polyethylenes by catalytic amination. *Science* **2023**, *381* (6665), 1433-1440. DOI: 10.1126/science.adg6093.
(21) Liu, K.; Zhao, Y.; Wolff, A. M.; Harry, K. L.; Rettner, E. M.; Miscall, J.; Rorrer, N. A.; Miyake, G. M. Repurposing Post-Consumer Polyethylene to Access Cross-Linked Polyethylene with Reprocessability, Recyclability, and Tunable Properties. *Angew. Chem. Int. Ed.* **2025**, *64* (19), e202502641. DOI: 10.1002/anie.202502641.
(22) Zeng, M.; Lee, Y.-H.; Strong, G.; LaPointe, A. M.; Kocen, A. L.; Qu, Z.; Coates, G. W.; Scott, S. L.; Abu-Omar, M. M. Chemical Upcycling of Polyethylene to Value-Added α,ω-Divinyl-Functionalized Oligomers. *ACS Sustain. Chem. Eng.* **2021**, *9* (41), 13926-13936. DOI: 10.1021/acssuschemeng.1c05272.
(23) Ellis, L. D.; Orski, S. V.; Kenlaw, G. A.; Norman, A. G.; Beers, K. L.; Román-Leshkov, Y.; Beckham, G. T. Tandem Heterogeneous Catalysis for Polyethylene Depolymerization via an Olefin-Intermediate Process. *ACS Sustain. Chem. Eng.* **2021**, *9* (2), 623-628. DOI: 10.1021/acssuschemeng.0c07612.
(24) Rachapudy, H.; Smith, G. G.; Raju, V. R.; Graessley, W. W. Properties of amorphous and crystallizable hydrocarbon polymers. III. Studies of the hydrogenation of polybutadiene. *Journal of Polymer Science: Polymer Physics Edition* **1979**, *17* (7), 1211-1222. DOI: 10.1002/pol.1979.180170706.
(25) Fastow, E. J.; Radzanowski, A. N.; Coughlin, E. B.; Winey, K. I. Increasing Branching and Functionalization Decreases Crystallinity and Crystallization Rate in Linear EVOH. *ACS Appl. Polym. Mater.* **2025**, *7* (3), 1618-1628. DOI: 10.1021/acsapm.4c03361.
(26) Gordon, B. M.; Parihar, A.; Hasanayn, F.; Goldman, A. S. High Activity and Selectivity for Catalytic Alkane–Alkene Transfer (De)hydrogenation by (tBuPPP)Ir and the Importance of

Choice of a Sacrificial Hydrogen Acceptor. *Organometallics* **2022**, *41* (22), 3426-3434. DOI: 10.1021/acs.organomet.2c00401.
(27) Kumar, A.; Bhatti, T. M.; Goldman, A. S. Dehydrogenation of Alkanes and Aliphatic Groups by Pincer-Ligated Metal Complexes. *Chem. Rev.* **2017**, *117* (19), 12357-12384. DOI: 10.1021/acs.chemrev.7b00247.
(28) Choi, J.; MacArthur, A. H. R.; Brookhart, M.; Goldman, A. S. Dehydrogenation and Related Reactions Catalyzed by Iridium Pincer Complexes. *Chem. Rev.* **2011**, *111* (3), 1761-1779. DOI: 10.1021/cr1003503.
(29) Böhmer, I. K.; Alt, H. G. Influence of triphenylphosphine on the activity of heterogeneous iridium, rhodium and platinum containing catalysts for the dehydrogenation of saturated hydrocarbons. *J. Organomet. Chem.* **2009**, *694* (7), 1001-1010. DOI: 10.1016/j.jorganchem.2008.07.010.
(30) Alt, H. G.; Böhmer, I. K. Catalytic Dehydrogenation of Isopentane with Iridium Catalysts. *Angew. Chem. Int. Ed.* **2008**, *47* (14), 2619-2621. DOI: 10.1002/anie.200704856.
(31) Taubmann, S.; Alt, H. G. Heterogeneous catalysts for the dehydrogenation of saturated hydrocarbons. *Journal of Molecular Catalysis A: Chemical* **2008**, *287* (1), 102-109. DOI: https://doi.org/10.1016/j.molcata.2008.02.023.
(32) Perras, F. A.; Arroyave, A.; Southern, S. A.; Lamb, J. V.; Li, Y.; LaPointe, A.; Delferro, M. Double-resonance 17O NMR experiments reveal unique configurational information for surface organometallic complexes. *Chem. Commun.* **2023**, *59* (31), 4604-4607, 10.1039/D3CC00899A. DOI: 10.1039/D3CC00899A.
(33) Kobayashi, T.; Perras, F. A.; Slowing, I. I.; Sadow, A. D.; Pruski, M. Dynamic Nuclear Polarization Solid-State NMR in Heterogeneous Catalysis Research. *ACS Catalysis* **2015**, *5* (12), 7055-7062. DOI: 10.1021/acscatal.5b02039.
(34) Lesage, A.; Lelli, M.; Gajan, D.; Caporini, M. A.; Vitzthum, V.; Miéville, P.; Alauzun, J.; Roussey, A.; Thieuleux, C.; Mehdi, A.; et al. Surface Enhanced NMR Spectroscopy by Dynamic Nuclear Polarization. *Journal of the American Chemical Society* **2010**, *132* (44), 15459-15461. DOI: 10.1021/ja104771z.
(35) Chen, L.; Wang, Q.; Hu, B.; Lafon, O.; Trébosc, J.; Deng, F.; Amoureux, J.-P. Measurement of hetero-nuclear distances using a symmetry-based pulse sequence in solid-state NMR. *Physical Chemistry Chemical Physics* **2010**, *12* (32), 9395-9405, 10.1039/B926546E. DOI: 10.1039/B926546E.
(36) Gullion, T.; Schaefer, J. Rotational-echo double-resonance NMR. *Journal of Magnetic Resonance (1969)* **1989**, *81* (1), 196-200. DOI: https://doi.org/10.1016/0022-2364(89)90280-1.
(37) Bennett, A. E.; Griffin, R. G.; Ok, J. H.; Vega, S. Chemical shift correlation spectroscopy in rotating solids: Radio frequency ‐ driven dipolar recoupling and longitudinal exchange. *J. Chem. Phys.* **1992**, *96* (11), 8624-8627. DOI: 10.1063/1.462267 (acccessed 2/25/2025).
(38) Ishii, Y. C13–C13 dipolar recoupling under very fast magic angle spinning in solid-state nuclear magnetic resonance: Applications to distance measurements, spectral assignments, and high-throughput secondary-structure determination. *J. Chem. Phys.* **2001**, *114* (19), 8473-8483. DOI: 10.1063/1.1359445 (acccessed 9/8/2025).
(39) Yang, X.-F.; Wang, A.; Qiao, B.; Li, J.; Liu, J.; Zhang, T. Single-Atom Catalysts: A New Frontier in Heterogeneous Catalysis. *Acc. Chem. Res.* **2013**, *46* (8), 1740-1748. DOI: 10.1021/ar300361m.
(40) It should be noted that there was some amount of unavoidable carryover of catalyst nanoparticles, inorganic nanoparticles can adhere to the column packing material, which when

'blended' with nonpolar polyethylene (i.e. HDPE) may result in the HDPE/SiO2 material having limited solubility resulting in peak fronting or adherence to the column resulting in peak tailing, both of which will result in broadening.
(41) Pitkänen, L.; Striegel, A. M. Size-exclusion chromatography of metal nanoparticles and quantum dots. *Trends Anal. Chem* **2016**, *80*, 311-320. DOI: 10.1016/j.trac.2015.06.013.
(42) Wahab, M. F.; Patel, D. C.; Armstrong, D. W. Total peak shape analysis: detection and quantitation of concurrent fronting, tailing, and their effect on asymmetry measurements. *J. Chromatogr. A* **2017**, *1509*, 163-170. DOI: 10.1016/j.chroma.2017.06.031.
(43) Knox, J. H. Practical Aspects of LC Theory. *J. Chromatogr. Sci.* **1977**, *15* (9), 352-364. DOI: 10.1093/chromsci/15.9.352 (acccessed 9/12/2025).